Wideband Channel Modeling for Wireless Avionics Intra-Communications

Jasper Brüggmann, Oscar Reyes, Christian Schappmann, Gerhard Bauch
Institute of Communications
Hamburg University of Technology
Hamburg, Germany
{jasper.brueggmann; oscar.reyes; christian.schappmann; bauch}@tuhh.de

***Abstract*—Wireless Avionics Intra-Communications (WAIC) has been proposed to partially replace costly wiring in future generations of aircraft. Besides the allocation of a frequency range and several performance figures, there is no standardized transmission scheme so far. For the design of suitable physical layer techniques, comprehensive models are required to perform realistic link-level simulations for the aircraft environment. This paper presents a wideband channel model for in-cabin WAIC systems, derived from channel measurements performed in an Airbus A321 cabin. The model is validated by comparing experimentally measured and simulated frame error rates using the proposed model in an IEEE 802.11a-based OFDM transmission.**

***Index Terms*—channel measurements, channel model, wireless avionics intra-communications, software-defined radio.**

I. Introduction

Introducing wireless communications in the aircraft cabin for digital avionics is envisioned to be one of the key enablers towards more economical and environmentally sustainable aviation. The reduction of cable mass, mounting hardware, maintenance and assembly cost, as well as dissimilar redundancy in combination with wired connections are the main incentives for the development of Wireless Avionics Intra-Communications (WAIC) [1]. A milestone towards a WAIC standard was reached, when the frequency band from $4.2\,\mathrm{GHz}$ to $4.4\,\mathrm{GHz}$ was allocated for WAIC. As radio altimeters providing safety-critical altitude measurements use the same frequency band, proper coexistence with WAIC has to be ensured. It has been recommended to limit the aggregate emissions of all WAIC nodes onboard an aircraft to $-20\,\mathrm{dBm}$ [2]. This constraint makes the selection of a suitable transmission scheme crucial, given the challenging propagation environment in the cabin. Furthermore, safety-critical WAIC applications usually have strict reliability and latency requirements.

As experimental physical layer design in hardware and measurements is often infeasible, a simulation framework resembling the propagation conditions in the cabin is a core element for the design of WAIC. The reliability of a transmission scheme can be assessed using link-level simulations. This requires a detailed model to account for the radio channel effects.

There have been several efforts to characterize the radio channel inside an aircraft cabin. In [3], the path loss and delay spread has been characterized for Ultra Wideband (UWB) communications within $3\,\mathrm{GHz}$ to $10.6\,\mathrm{GHz}$ in a Boeing 737-200 cabin. The authors extended their work in [4] by developing a small-scale fading model. In [5] they investigated the effect of passengers on the channel model. The mentioned works focus on UWB, that requires slightly different modeling approaches, e.g. frequency-dependent path loss and careful characterization of the fading statistics [6]. Only few studies target the channel characteristics specifically for WAIC. In [7], the authors assumed WAIC operating in frequency bands around $2.4\,\mathrm{GHz}$ and $5.8\,\mathrm{GHz}$, since the $4.3\,\mathrm{GHz}$ band had not been specified yet. [8] focuses on WAIC in the correct band onboard a light aircraft, measuring channel characteristics and error rates of an IEEE 802.11-based transmission. To the best of our knowledge, there are no works that connect channel measurements, stochastic channel modeling, link-level simulations and physically measured error rates for in-cabin WAIC in a single-aisle passenger aircraft. The contributions of this work can be summarized as follows:

- In Section II, the results of an in-cabin channel measurement campaign are presented. A comprehensive channel model is proposed for in-cabin WAIC systems that can be used for link-level simulations.
- Section III validates the developed channel model experimentally by comparing simulated frame error rates to in-cabin measurements using a Software-Defined Radio (SDR) platform. An Orthogonal Frequency Division Multiplexing (OFDM) transmission chain based on IEEE 802.11a is employed.

II. Channel Characterization

The channel measurements described in this section were conducted in a retired Airbus A321 cabin on the premises of the Finkenwerder Airbus site. This single-aisle cabin was equipped with three-seat rows on each side of the aisle, overhead compartments, monuments such as lavatories and galleys, ceiling panels, etc. The effects of luggage, passengers or moving objects are not in the scope of this paper. For each measurement, the single-antenna transmitter has been placed below the ceiling close to the starboard front door. This is assumed to be a likely mounting position for the access point in a WAIC network, as it is close to the central electronics compartment. The single-antenna receiver has been positioned below the overhead compartments at different positions along

the cabin, simulating the position of a WAIC endpoint. All measurements target the WAIC band within 4.2 GHz to 4.4 GHz. Since no antennas are commercially available for this band, custom dipole antennas provided by Airbus were used. Two distinct measurement setups have been used for the investigations, that will be presented in the following.

A. Vector Network Analyzer Setup

To perform meaningful link-level simulations even at high transmission bandwidths, the channel model has to describe small-scale fading effects that are mainly caused by multipath propagation. A series of measurements has been taken to assess this modeling part. Therefore, the two-port Vector Network Analyzer (VNA) function of a Rohde & Schwarz FSH-8 spectrum analyzer has been used to measure the discrete-frequency complex transmission coefficient $S_{21}(f)$, which directly translates to the complex channel transfer function $H_s(f) = S_{21}(f)/S_{21}^{\text{ref}}(f)$ at some receiver position s, with a wired reference measurement $S_{21}^{\text{ref}}(f)$.

To reduce the measurement noise, $H_s(f)$ results from averaging 20 frequency sweeps. Since transmit and receive antenna must be connected to the VNA, the measurement distance d is limited by the cable length. Due to the lack of an amplifier and longer cables, the maximum distance was limited to approximately 6 m. Here, 220 MHz have been captured around 4.3 GHz. The receiver position has been varied along the cabin by selecting every other row of seats on both sides of the aisle, which we refer to as global position. To capture sufficient statistics of the small-scale fading effects, the receiver position has been varied by 5 cm in direction of the seat row at each global position, leading to 9 local positions per global position. Additionally, two antennas placed 16 cm apart were selectable using a switch at both transmitter and receiver, resulting in 4 measurements per local position and 36 measurements per global position.

B. Small-Scale Channel Effects

Indoor radio channels are commonly modeled using the Saleh-Valenzuela model [9], assuming that the multipath components arrive at the receiver in clusters with doubly exponential Power Delay Profile (PDP). In industrial indoor environments [6] as well as aircraft cabins [10] where the scatterers are densely spaced, it has been observed that the clusters collapse into a single exponential cluster. As it will be shown below, the measurements of this work share this observation. Thus, every resolvable delay bin can be assumed to contain significant energy and the Channel Impulse Response (CIR) is described by $h(\tau) = \sum_{k=0}^{\infty} a_k \delta(\tau - \tau_k)$ with $h(\tau) = 0$ for $\tau < 0$, $a_k \in \mathbb{C}$ and $\tau_k = k/B$. This dense cluster model has unit-energy exponential average PDP with time constant γ

$$E\{|a_k|^2\} = \frac{1\,\text{s}}{\gamma} \exp\left(-\frac{\tau_k}{\gamma}\right). \tag{1}$$

As described in Section II-A, several $H_s(f)$ have been measured in the aircraft cabin. These can be converted to discrete-time CIRs described by a_k^s via inverse Fourier transformation, from which the PDP $|a_k^s|^2$ can be computed. Some exemplary PDPs are shown in Fig. 1. Note that the measured PDPs have been shifted in time by d/c_0 to account for the propagation time of the direct path, where c_0 is the speed of light. It becomes apparent that each resolvable delay bin contains significant energy and that the PDPs in dB decay linearly before reaching the noise floor.

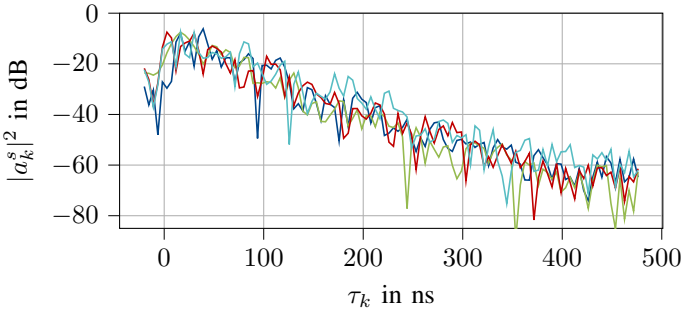

Fig. 1. Exemplary measured power delay profiles for $d \approx 6\,\text{m}$.

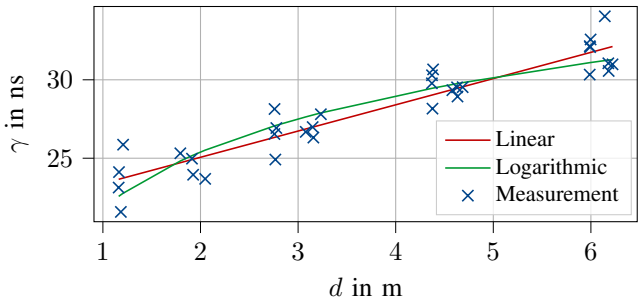

Fig. 2. Measured time constants γ and corresponding model fits.

Using these measured PDPs, the resulting spatially averaged PDPs along the cabin have been analyzed. To avoid the noise floor, the average PDPs have been truncated such that only $\tau \in [0, \tau_{\max}]$ is considered where $\tau_{\max}$ is chosen where the average PDP decays below a power threshold of $-40\,\text{dB}$ versus its maximum. The resulting γ has been determined as shown in Fig. 2 using linear regression. We observe an increase with d, thus the PDP decays slower at high distances and frequency selectivity gets more severe. The time constant can be modeled to depend linearly on the distance d [10]:

$$\gamma = \gamma_0 + \frac{m_\gamma d}{1\,\text{m}} + X_\gamma. \tag{2}$$

Here, $X_\gamma \sim \mathcal{N}(0, \sigma_\gamma^2)$ is a random term to account for modeling errors. Alternatively, γ could be modeled to increase logarithmically with d [4] as

$$\gamma = \gamma_0 + 10 m_\gamma \log_{10}\left(\frac{d}{1\,\text{m}}\right) + X_\gamma. \tag{3}$$

The parameters found for these two models are given in Table I, in addition to the comparable results of [4], [10]. As σ_γ quantifies the modeling error, the linear model turns out to be a slightly better fit compared to the logarithmic model.

To complete the small-scale fading channel model, the statistics of the channel coefficients a_k have to be characterized. Literature suggests many possible distributions of

TABLE I
SMALL-SCALE MODEL PARAMETERS. THE SELECTED MODEL IS HIGHLIGHTED IN GRAY.

Model	γ_0 in ns	m_γ in ns	σ_γ in ns
Linear	21.714	1.673	1.077
Logarithmic	21.788	1.197	1.207
Linear [10]	14.74	2.28	5.66
	...	...	...
	16.68	3.26	9.40
Logarithmic [4]	12.7	1.10	0.648
	...	...	...
	16.02	1.54	1.22

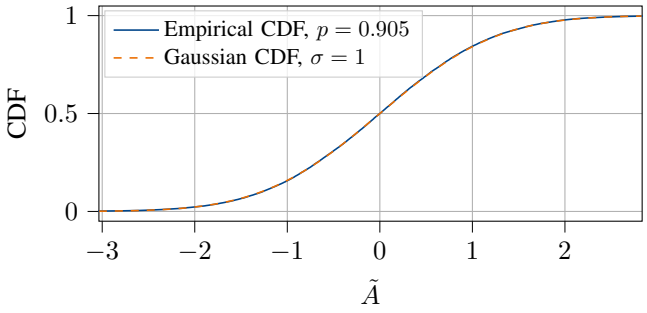

Fig. 3. Cumulative distribution function of the normalized fading dimensions.

the magnitudes $|a_k|$ such as Nakagami, Rayleigh, Rice or Weibull distributions [4], [6], [10]. The Nakagami distribution is frequently used, as it can be seen as a generalization of Rayleigh and Rice distributions [10]. The mentioned literature focuses on UWB where a delay bin often only contains a few multipath components. Consequently, the central limit theorem cannot be applied anymore and the fading coefficients cannot be assumed to be Rayleigh distributed [6]. However, the 200 MHz WAIC bandwidth is relatively small with an actual signal most likely occupying only a fraction of the available band. Thus, we assume that the central limit theorem still holds. Consequently, we expect a_k to be complex Gaussian, i.e. $a_k \sim \mathcal{CN}(0, \frac{1}{2}E\{|a_k|^2\})$. To jointly verify the Gaussian nature of the channel coefficients, the measured a_k can be normalized, such that

$$\tilde{a}_k = \frac{a_k}{\sqrt{\frac{1}{2}E\{|a_k|^2\}}} = \tilde{a}_k^{\text{re}} + j\tilde{a}_k^{\text{im}}. \tag{4}$$

In the next step, all measured $\tilde{a}_k^{\text{re}}$ and $\tilde{a}_k^{\text{im}}$ are considered to be realizations of a random variable $\tilde{A}$. As shown in Fig. 3, the empirical Cumulative Distribution Function (CDF) of $\tilde{A}$ aligns well with a standard normal CDF. Carrying out a Kolmogorov-Smirnov test proves the alignment of measured and assumed CDF with a p-value of 0.905.

C. Coherence Bandwidth

Characterizing the frequency selectivity of a channel in terms of the coherence bandwidth B_c is a well-known problem, as it can help in selecting an appropriate transmission scheme. It can be computed using the frequency correlation $\Phi(\Delta f) = \mathcal{F}\left[E\left\{|a_k|^2\right\}\right]$ [11] with discrete Fourier transform $\mathcal{F}[\cdot]$. B_c is defined as the frequency separation Δf, where

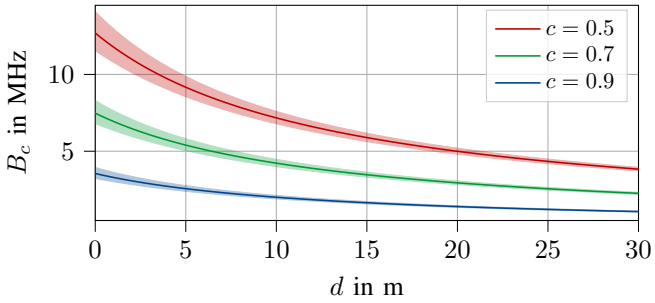

Fig. 4. Coherence bandwidth with frequency correlation threshold c.

two points in the frequency domain are sufficiently decorrelated. Thus, a correlation threshold c has to be defined, giving $B_c = \min(\Delta f)$, where $|\Phi(\Delta f)| = c$. Using Eq. (1), we can compute $\Phi(\Delta f) = (1 + j2\pi\Delta f\gamma)^{-1}$. An analytical expression of the coherence bandwidth is then given by

$$B_c = (2\pi\gamma)^{-1}\sqrt{c^{-2} - 1}. \tag{5}$$

It is noteworthy, that γ is equal to the RMS delay spread τ_{rms} [11] of $E\left\{|a_k|^2\right\}$ given by Eq. (1), yielding the more common notion of B_c being anti-proportional to τ_{rms}.

Based on Eq. (5) and Eq. (2), the distance-dependent B_c has been evaluated in Fig. 4. The shaded areas mark the 95% confidence interval based on σ_γ. It can be seen, that B_c decreases with increasing distance, resulting in a values below 5 MHz after 20 m for $c = 0.5$. In order to achieve reliable communication through frequency diversity, the WAIC signal should occupy multiple B_c.

D. Software-Defined Radio Setup

The VNA setup described in Section II-A is mainly suitable to measure small-scale channel effects in the front of the cabin. As WAIC is assumed to use very low transmit power, the transmission range will be mainly limited by path loss and noise. Therefore, another setup is required to characterize the large-scale channel effects along the whole cabin. A low-cost solution can be realized using SDRs. The SDR setup described in this section has been assembled to measure Frame Error Rate (FER) as presented in Section III. However, the measurements can be analyzed in terms of large-scale channel effects as well.

In this work, two Ettus USRP B210 were used to transmit and receive a 20 MHz-wide OFDM waveform based on IEEE 802.11a in the WAIC band with 0 dBm transmit power. In Section III, the FER is measured with this setup by transmitting a stream of 256 known packets for each experiment with -20 dBm transmit power. For measuring path loss, only the received IQ samples r_k^{sync} after synchronization are required. Synchronization as in [12] is achieved by exploiting the preamble and pilots. To capture multiple channel realizations at every global position, a grid of 6 positions with 5 cm spacing is applied. Each measurement is repeated at three carrier frequencies $f_c \in \{4.22\,\text{GHz}, 4.3\,\text{GHz}, 4.38\,\text{GHz}\}$, resulting in 18 measurements per global position. Similarly to Section II-A, a wired reference measurement r_k^{ref} is necessary to estimate the path loss. During the wired measurement, 60 dB

attenuation A_{ref} was applied to prevent receiver saturation. To reduce measurement noise and small-scale fading effects, the measured path loss $L(d)$ for each global position is obtained by averaging over all local positions and carrier frequencies:

$$L(d) = 10\log_{10}\left(\frac{1}{18}\sum_{s,f_c}\frac{\sum_k |r_k^{\text{sync}}|^2}{A_{\text{ref}}\sum_k |r_k^{\text{ref}}|^2}\right)\text{dB}. \quad (6)$$

For each global position, the associated distance d is the average distance of all 6 local positions.

E. Large-Scale Channel Effects

An essential part of a wireless channel model is the characterization of large-scale effects, namely path loss and shadow fading. These aspects are typically modeled using a log-linear relationship, depending on the distance d between transmitter and receiver:

$$L(d) = X_L - L_0 - 10n_0\log_{10}\left(\frac{d}{1\,\text{m}}\right)\text{dB}. \quad (7)$$

Here, n_0 is the path loss exponent and $X_L \sim \mathcal{N}(0,\sigma_L^2)$ denoting a Gaussian shadowing term. Note that we assume no frequency dependence since the WAIC bandwidth of 200 MHz is relatively small. We measure large-scale fading using the SDR setup described in Section II-D.

Fig. 5 provides the measured path loss at several distances within 1.6 m to 30.5 m. The measurements do not show a purely log-linear increase over d as Eq. (7), but an increasing slope can be observed. To find a suitable path loss model, two alternative formulations are considered. Firstly, an uncommon log-quadratic relation is considered, that has been selected purely by visual inspection of the measurement data:

$$L(d) = X_L - L_0 - 10n_0\left[\log_{10}\left(\frac{d}{1\,\text{m}}\right)\right]^2\text{dB}. \quad (8)$$

More commonly known is a segment-wise log-linear model:

$$L(d) = X_L + \begin{cases} -L_0 - 10n_0\log_{10}\left(\frac{d}{1\,\text{m}}\right)\text{dB}, & d \le d_{\text{B}} \\ -L_1 - 10n_1\log_{10}\left(\frac{d}{1\,\text{m}}\right)\text{dB}, & d > d_{\text{B}} \end{cases}, \quad (9)$$

with $L_1 = L_0 + 10(n_0 - n_1)\log_{10}\left(\frac{d_{\text{B}}}{1\,\text{m}}\right)$ dB. We refer to this as breakpoint model, because the path loss exponent varies at a certain breakpoint distance d_{B}.

Parameterizations have been found via least-squares fitting as displayed in Fig. 5. The results are summarized in Table II. Note that σ_L corresponds to the root-mean-square error of the fitting. Clearly, the breakpoint model yields the smallest error $\sigma_L = 0.93$ dB and will thus be selected for the remainder of this paper. Similar parameterizations of the breakpoint model have been found in [10] as shown in Table II as well.

Fig. 6 shows the empirically computed CDF of the measured shadowing term X_L as well as a Gaussian CDF with the resulting $\sigma_L = 0.93$ dB, visualizing the quasi-Gaussian distribution of X_L.

Note that this large-scale model has been acquired for an unoccupied cabin. In case passengers and luggage are present, the path loss and shadowing behavior will most likely be more severe [5].

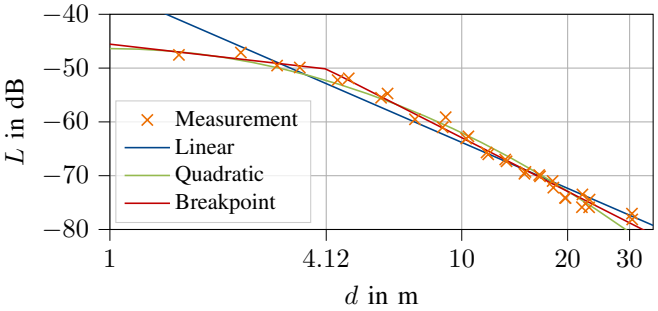

Fig. 5. Path loss measurement and fits resulting from different models.

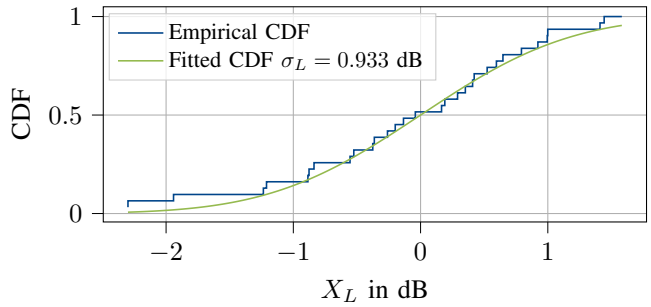

Fig. 6. Shadowing CDF resulting from breakpoint path loss model.

With that, a complete channel model for single-antenna link-level simulations can be implemented. The model parameters that will be used in the remainder of this work are highlighted in Table I and Table II.

III. Experimental Model Validation

This section aims at validating the channel model developed in Section II by comparing simulated FER using the model to experimentally measured FER. For that, an OFDM transmission chain based on IEEE 802.11a with varying bandwidth B, BPSK modulation and convolutional code rate 1/2 is used. The simulations have been conducted using the open source library Sionna [13], as well as custom components for synchronization and the channel. The measurement setup described in Section II-D is used. After a pre-processing step parallelizing the serially received packets, the IQ samples are demodulated offline using the same code as the simulation.

A. System Model and Error Rate Results

In addition to the channel model of Section II, some physical impairments have been applied in simulation. As illustrated

TABLE II
Large-scale model parameters. The selected model is highlighted in gray.

Model	L_0 in dB	n_0	n_1	d_{B} in m	σ_L in dB
Linear	35.44	2.83	-	-	1.84
Quadratic	46.37	1.56	-	-	1.34
Breakpoint	45.55	0.75	3.32	4.12	0.93
Breakpoint [10]	40.45	-0.08	2.27	2.84	1.76
	...	...	...	...	...
	46.72	1.51	3.19	7.24	2.74

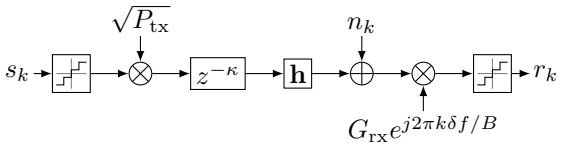

Fig. 7. Extended channel model with physical impairments.

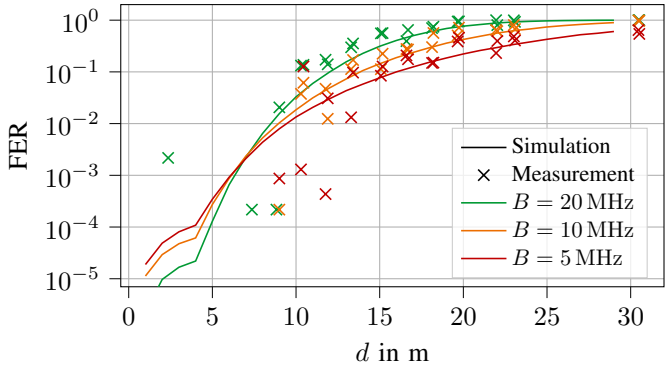

Fig. 8. Error rate performance of measurement and simulation.

in Fig. 7, the transmit signal s_k is processed by a 12-bit digital-to-analog converter, modeled by a uniform mid-rise quantization with maximum input level of ± 5. The transmit power P_{tx} is set to $-20\,\mathrm{dBm}$. To introduce a timing offset, the signal is then delayed by κ samples. After convolution with the generated discrete CIR $\mathbf{h}$ including multiplicative path loss, AWGN with power $P_N = k_{\mathrm{B}}TBF$ is added. Here, k_{B} denotes the Boltzmann constant, $T = 298.15\,\mathrm{K}$ and $F = 9\,\mathrm{dB}$ is the experimentally found noise figure. Subsequently, a carrier frequency offset $\delta f = 10\,\mathrm{kHz}$ and $76\,\mathrm{dB}$ receiver gain G_{rx} is applied before 12-bit mid-rise analog-to-digital conversion.

Synchronization as in [12] was achieved, exploiting the IEEE 802.11a preamble and pilot subcarriers. Channel estimation is performed using the long training sequence of the preamble. A soft-decision Viterbi decoder performs forward error correction.

Fig. 8 compares the FERs measured in the aircraft cabin to corresponding FER simulations, using the channel model developed in this work. As the model includes path loss and the simulation aims to imitate the measurement procedure, the FER is shown depending on the distance d. Similarly to Section II-D, the FER across all 256 packets is computed at every local position. The measurements in Fig. 8 result from spatially averaging the FER at every global position.

It can be observed, that the simulated FER decays below 10^{-3} for $d < 6\,\mathrm{m}$. Except for one outlier, the measured FER is zero for $d < 8\,\mathrm{m}$ with limited statistics. Presumably, the measurements would get closer to the simulation results in this low-FER region with more independent measurements at hand. Overall, the simulated and measured FERs agree very well up to a few meters. This verifies the channel model for in-cabin WAIC physical layer design.

IV. Conclusions

This work presented the results of a measurement campaign, characterizing the propagation environment inside an Airbus A321 aircraft cabin. The transmitter and receiver positions have been chosen according to a likely deployment of a WAIC network. A stochastic large- and small-scale channel model has been derived and implemented in simulation. Finally, the channel model has been verified by showing that the simulated FER agrees well with SDR-based FER measurements. For that, an IEEE 802.11a-based transmission chain has been used in the WAIC frequency band with a low transmit power of $-20\,\mathrm{dBm}$. This low-power physical layer only achieved small transmission ranges at high reliability. In future work, the channel model can be used to design a more robust physical layer to meet the requirements of WAIC.

Acknowledgment

This work was funded by the German Federal Ministry for Economic Affairs and Climate Action (BMWK) within the project DaKliF (grant agreement number 20Y2202D). The measurement environment and equipment was provided by Airbus Operations GmbH, along with their general support.

References

[1] P. Park, P. Di Marco, J. Nah, and C. Fischione, "Wireless Avionics Intracommunications: A Survey of Benefits, Challenges, and Solutions," *IEEE Internet of Things Journal*, vol. 8, no. 10, pp. 7745–7767, May 2021.

[2] ICAO, "Proposed Amendment to the International Standards and Recommended Practises, Aeronautical Telecommunications, Annex 10, Vol. V, Aeronautical Radio Frequency Spectrum Utilization to the Convention on International Civil Aviation," Jun. 2023.

[3] J. Chuang, N. Xin, H. Huang, S. Chiu, and D. G. Michelson, "UWB Radiowave Propagation within the Passenger Cabin of a Boeing 737-200 Aircraft," in *2007 IEEE 65th Vehicular Technology Conference - VTC2007-Spring*, Apr. 2007, pp. 496–500, iSSN: 1550-2252.

[4] S. Chiu, J. Chuang, and D. G. Michelson, "Characterization of UWB Channel Impulse Responses Within the Passenger Cabin of a Boeing 737-200 Aircraft," *IEEE Transactions on Antennas and Propagation*, vol. 58, no. 3, pp. 935–945, Mar. 2010.

[5] S. Chiu and D. G. Michelson, "Effect of Human Presence on UWB Radiowave Propagation Within the Passenger Cabin of a Midsize Airliner," *IEEE Transactions on Antennas and Propagation*, vol. 58, no. 3, pp. 917–926, Mar. 2010.

[6] A. Molisch, "Ultrawideband propagation channels-theory, measurement, and modeling," *IEEE Transactions on Vehicular Technology*, vol. 54, no. 5, pp. 1528–1545, Sep. 2005.

[7] H. Saghir, C. Nerguizian, J. J. Laurin, and F. Moupfouma, "In-Cabin Wideband Channel Characterization for WAIC Systems," *IEEE Transactions on Aerospace and Electronic Systems*, vol. 50, no. 1, pp. 516–529, Jan. 2014.

[8] I. Bang, H. Nam, W. Chang, T. Kim, J.-M. Woo, C.-Y. Kim, T.-W. Ban, P. Park, and B. C. Jung, "Channel Measurement and Feasibility Test for Wireless Avionics Intra-Communications," *Sensors*, vol. 19, no. 6, p. 1294, Jan. 2019.

[9] A. Saleh and R. Valenzuela, "A Statistical Model for Indoor Multipath Propagation," *IEEE Journal on Selected Areas in Communications*, vol. 5, no. 2, pp. 128–137, Feb. 1987.

[10] M. Bachhuber, "Analysis and Modeling of Radio Propagation in Passenger Cabins of big sized Aircrafts," Ph.D. dissertation, Friedrich-Alexander University Erlangen-Nürnberg (FAU), Apr. 2011. [Online]. Available: https://open.fau.de/handle/openfau/1701

[11] M. Varela and M. Sanchez, "RMS delay and coherence bandwidth measurements in indoor radio channels in the UHF band," *IEEE Transactions on Vehicular Technology*, vol. 50, no. 2, pp. 515–525, Mar. 2001.

[12] T. Schmidl and D. Cox, "Robust frequency and timing synchronization for OFDM," *IEEE Transactions on Communications*, vol. 45, no. 12, pp. 1613–1621, Dec. 1997.

[13] J. Hoydis, S. Cammerer, F. Ait Aoudia, M. Nimier-David, L. Maggi, G. Marcus, A. Vem, and A. Keller, "Sionna," 2022. [Online]. Available: https://nvlabs.github.io/sionna/